Journal of Solid State Chemistry 183 (2010) 157–167

Contents lists available at ScienceDirect

Journal of Solid State Chemistry

journal homepage: www.elsevier.com/locate/jssc

(Ca/Sr)Au_xCd_{1-x}: Stacking variants of the CrB–FeB series

Wiebke Harms, Ines Dürr, Michael Daub, Caroline Röhr *

Institut für Anorganische und Analytische Chemie, University of Freiburg, Albertstr. 21, D-79104 Freiburg, Germany

ARTICLE INFO

Article history:
Received 11 August 2009
Received in revised form
16 October 2009
Accepted 25 October 2009
Available online 31 October 2009

PACS:
61.66.Fn
71.20.Lp

Keywords:
Aurides
Cadmides
Crystal structure
Band structure calculation

ABSTRACT

The structural chemistry of binary 1:1 alkaline earth metallides $A^{II}M$ (M = p−block or late transition element) is dominated by planar M zig-zag chains, which are stacked in different orientations (CrB (c) to FeB (h) type) and with variable stacking distances (types I and II). As a case study of the electronic influences, the substitution of Au against Cd in the respective Ca and Sr aurides was examined by means of experimental, crystallographic and computational methods. Starting from CaAu, up to 11% of Au can be substituted by Cd without a change in the CrB structure type (orthorhombic, space group *Cmcm*, $a = 398.2(1)$, $b = 1122.6(6)$, $c = 460.9(2)$ pm, $Z = 4$, $R1 = 0.0303$). Starting from SrAu (stacking sequence $(hc)_2(h_2c)_2$), depending on the proportion of the Cd substitution a successive change to structures with increased hexagonality is observed: In $SrAu_{0.93}Cd_{0.07}$ (monoclinic, space group $P2_1/m$, $a = 621.3(4)$, $b = 472.4(2)$, $c = 1216.1(9)$ pm, $\beta = 96.97(5)^\circ$, $Z = 6$, $R1 = 0.0467$) the stacking sequence is h_{2c}, i.e. the hexagonality is 66.67%. A slightly more increased Cd content in $SrAu_{0.78}Cd_{0.22}$ (orthorhombic, space group *Pnma*, $a = 3243.3(8)$, $b = 474.17(8)$, $c = 626.20(9)$ pm, $Z = 16$, $R1 = 0.0682$) drives the hexagonality to 75%, with a $(h_3c)_2$ stacking sequence known from several rare earth nickel compounds. Further Cd substitution is not possible. However, in the Cd-rich section of the two series, where the CsCl/β−brass structure type occurs for both alkaline earth elements, a small Au substitution, as determined from powder data by Rietveld refinements, is possible. The substitution limit and the stability ranges of the CsCl and the CrB type can be rationalized from the calculated band structures. Geometrical and electronic criteria are used to compare and discuss the stability ranges in a structural map.

1. Introduction

The structural chemistry of binary 1:1 alkaline earth metallides $A^{II}M$ (M = p−block or late transition element) is dominated by planar M zig-zag chains, which are stacked in different orientations (CrB- to FeB-type) and with variable stacking distances (type I and II). The change from the CrB-I type (stretched trigonal A prisms around M) to the respective type II structures (compressed prisms), driven by the valence electron concentration (v.e.c.), is already discussed in the literature [1,2] and has recently been examined in more detail for the phase width AM^{14} (v.e./$M = 6$)−AM^{13} (v.e./$M = 5$) by means of crystallographic and computational studies [3]. CaGa is the only compound of this structure family with v.e./$M = 5$, while the binary monoindides [4] and mixed trielides [5] form other singular structures. For the compounds $A^{II}Zn$ with v.e./$M = 4$, the structures change from the CrB-II type (CaZn [6]) to the FeB-II type (SrZn [1]) or the simple CsCl type of BaZn [7] is obviously driven by the decreasing radius ratio r_M/r_A. On the other hand, in the silver series (CaAg: CrB-II [1]–SrAg: dimorphic with two complicated stacking variants [8]–BaAg: FeB-II [8]), i.e. at v.e./$M = 3$, five different stacking variants have been observed [9]. In this case, the successive change from pure cubic (CrB-II) to exclusively hexagonal stacking (FeB-II) is also obviously caused by the change of the radius ratio. Similar size-dependent CrB–FeB stacking series have been observed for the *Ln*Ni binary and ternary intermetallics (v.e./$M = 3.0$) [10–12]. For a case study of the electronic influences, the substitution of Au against Cd in the respective Ca and Sr aurides was chosen over the argentides as a differentiation of Ag and Cd via X-ray diffraction methods is not possible. Argentides and aurides (CaAu: CrB-II [1]–SrAu: singular structure type with 60% hexagonality [8]) show a comparable radii dependent stacking sequence change (although possible stacking variants inbetween are not yet confirmed for the aurides) and a broad variety of stacking variants is already known for the series CaCu−CaM (M = Ga [13], Zn [14], Ge [13], etc.), CaAg–CaZn [15], SrAg–SrZn [13] and SrCu–SrCd [16].

2. Experimental section

2.1. Preparation

The synthesis of the title compounds was generally performed starting from the elements calcium or strontium, cadmium and gold obtained from commercial sources and used without further purification (Ca: Aldrich, 99%; Sr: Metallhandelsgesellschaft

* Corresponding author.
E-mail address: caroline@ruby.chemie.uni-freiburg.de (C. Röhr).

0022-4596/$ - see front matter © 2009 Elsevier Inc. All rights reserved.
doi:10.1016/j.jssc.2009.10.027

Maassen, Bonn, 99%; Au: Heraeus GmbH, 99.99% and Cd: ABCR Karlsruhe, 99.999%). The educts were filled into tantalum crucibles under an argon atmosphere. The sealed containers were heated in corundum tubes under a static Ar atmosphere to a maximum temperature of 1375 K with constant heating/cooling rates given in Table 1 for all samples. Representative parts of the reguli were ground and sealed in capillaries with a diameter of 0.3 mm. X-ray powder diagrams were collected on a transmission powder diffractometer system (STADI P, linear PSD, Fa. Stoe & Cie, Darmstadt, MoK_α radiation, graphite monochromator).

For the Ca series, four samples were prepared along the section $CaAu_xCd_{1-x}$. In all cases the powder patterns of the samples showed the formation of 1:1 compounds exclusively: For Au contents x between 0.1 and 0.3, the CsCl type structures are formed in pure phase, however with very low crystal qualities. For that reason, a Rietveld refinement of the X-ray powder pattern was preferred to a single crystal structure determination. In all cases the Au/Cd proportion of the statistically occupied positions fits the sample composition. At a 1:1 proportion of Au:Cd, the sample contains both the most Au-rich compound with the CsCl structure type, $CaAu_{0.29}Cd_{0.71}$, and the most Cd-rich phase with the CrB structure type, $CaAu_{0.89}Cd_{0.11}$. This product composition thus nicely demonstrates the phase width of the CsCl (Cd-rich) and the CrB type (Au-rich) structure. Also, the fact that in samples with a Au content of 80% small amounts of the CsCl type can be identified from the powder diffraction diagram confirms the mentioned composition ranges of the two structure types.

In the case of the respective strontium series, the powder pattern of the Au-rich sample of composition $SrAu_{0.8}Cd_{0.2}$ can be fully indexed using the theoretical diffraction diagram of the monoclinic phase $SrAu_{0.93}Cd_{0.07}$ (crystal data see Tables 3 and 4). Evidently, in this case a small loss of cadmium occurs, which can be easily explained from the high volatility of Cd. In the Cd-rich samples with

Table 1
Details of the synthesis of the Ca/Sr–Au–Cd compounds.

Sample composition	Weighted sample						T program			Phase composition from powder data (structure type)
	A		Au		Cd		$\dot{T}\uparrow$ (K/h)	T_{max} (K)	$\dot{T}\downarrow$ (K/h)	
	mg	mmol	mg	mmol	mg	mmol				
$CaAu_{0.8}Cd_{0.2}$	182.6	4.56	714.8	3.63	102.2	0.91	30	1375	20	$CaAu_{0.9}Cd_{0.1}$ (CrB)
$CaAu_{0.5}Cd_{0.5}$	206.3	5.15	505.4	2.57	289.2	2.57	30	1375	20	$CaAu_{0.89}Cd_{0.11}$ (CrB); $CaAu_{0.29}Cd_{0.71}$ (CsCl)
$CaAu_{0.3}Cd_{0.7}$	225.2	5.62	333.1	1.69	442.8	3.94	200	1375	20	$CaAu_{0.29}Cd_{0.71}$ (CsCl)
$CaAu_{0.1}Cd_{0.9}$	249.6	6.23	123.0	0.62	628.9	5.59	200	1375	20	$CaAu_{0.13}Cd_{0.87}$ (CsCl)
$SrAu_{0.8}Cd_{0.2}$	328.1	3.74	588.0	2.96	84.1	0.75	200	1375	20	$SrAu_{0.93}Cd_{0.07}$ ($Y_{0.3}Gd_{0.7}Ni$)
$SrAu_{0.5}Cd_{0.5}$	362.2	4.13	405.8	2.04	231.3	2.06	200	1375	20	$SrAu_{0.92}Cd_{0.08}$ ($Y_{0.3}Gd_{0.7}Ni$), $SrCd_2$
$SrAu_{0.2}Cd_{1.8}$	399.1	4.55	179.4	0.90	921.6	8.20	200	1375	10	$SrAu_{0.78}Cd_{0.22}$ ($CaCu_{0.8}Zn_{0.2}$), $SrCd_2$

Table 2
Crystallographic data, details of the data collection and structural determination for the compounds $CaAu_{0.89}Cd_{0.11}$, $CaAu_{0.29}Cd_{0.71}$ and $CaAu_{0.13}Cd_{0.87}$.

Compound	$CaAu_{0.89}Cd_{0.11}$		$CaAu_xCd_{1-x}$	
x	0.89	0.29(2)		0.13(1)
Structure type	CrB-II		CsCl	
Stacking sequence	c		–	
Hexagonality (%)	0		–	
Crystal system	Orthorhombic		Cubic	
Space group	$Cmcm$, no. 63		$Pm\bar{3}m$, no. 221	
Lattice constants (pm)				
a	397.7(2)	378.15(7)		382.29(4)
b	1122.7(6)		–	
c	461.5(1)		–	
Volume of the u.c. (10^6 pm^3)	206.0	54.07(3)		55.87(2)
Z	4		1	
Density (X-ray) (g/cm^3)	7.29	5.43		4.86
Diffractometer	Stoe IPDS-2		Stoe STADI-P	
	Mo$K\alpha$ radiation, graphite monochromator			
Absorption coeff. $\mu_{MoK\alpha}$ (mm^{-1})	65.61	–		–
θ range (deg)	3.6–27.8		4.0–40.0	
No. of reflections collected	1303	–		–
No. of independent reflections	156		28	
R_{int}	0.0854	–		–
Corrections	Lorentz, polarization, absorption			
Refinement	SHELXL-97 [18]		GSAS [20]	
No. of free parameters	10		22	
Goodness-of-fit on F^2	1.119		–	
R values (for refl. with $I \geq 2\sigma(I)$)				
$R1$	0.0308	$R_I = 0.0778$		$R_I = 0.0268$
$wR2$	0.0733	$R_p = 0.0578$		$R_p = 0.0499$
R values (all data)				
$R1$	0.0308		–	
$wR2$	0.0733		–	
Residual elect. density (e$^-$ 10^{-6} pm^{-3})	2.0/−1.8		–	

Au contents x of 0.5 to 0.2 the binary dicadmide $SrCd_2$ [17] is formed in addition to the two new 1:1 compounds $SrAu_{0.93}Cd_{0.07}$ ($Y_{0.3}Gd_{0.7}Ni$ type) and $SrAu_{0.78}Cd_{0.22}$ ($CaCu_{0.8}Zn_{0.2}$ type).

Table 3
Crystallographic data, details of the data collection and structural determination for the compounds $SrAu_{0.93}Cd_{0.07}$ and $SrAu_{0.78}Cd_{0.22}$.

Compound	$SrAu_{0.93}Cd_{0.07}$	$SrAu_{0.78}Cd_{0.22}$
Structure type	$Gd_{0.7}Y_{0.3}Ni$ [10]	$CaCu_{0.8}Zn_{0.2}$ [14]
Stacking sequence	h_2c	$(h_3c)_2$
Hexagonality (%)	66.67	75
Crystal system	Monoclinic	Orthorhombic
Space group	$P2_1/m$, no. 11	*Pnma*, no. 62
Lattice constants (pm, °)		
a	621.3(4)	3243.3(8)
b	472.4(2)	474.17(8)
c	1216.1(9)	626.20(9)
β	96.97(5)	–
Volume of the u.c. (10^6 pm^3)	354.3(4)	963.0(3)
Z	6	16
Density (X-ray) (g/cm^3)	7.83	7.36
Diffractometer	Stoe IPDS-2	
	MoK_α radiation, graphite monochromator	
Absorption coeff $\mu_{MoK\alpha}$ (mm^{-1})	80.8	71.52
θ range (deg)	1.7–26.2	2.5–29.3
No. of reflections collected	4464	6657
No. of independent reflections	790	1359
R_{int}	0.1390	0.1507
Corrections	Lorentz, polarization, absorption	
Structure solution	Shelxs-97 [42]	
Refinement	Shelxl-97 [18]	
No. of freeparameters	41	54
Goodness-of-fit on F^2	1.108	0.875
R values (for refl. with $I \geq 2\sigma(I)$)		
*R*1	0.0467	0.0682
*wR*2	0.1141	0.1904
R values (all data)		
*R*1	0.0616	0.1825
*wR*2	0.1207	0.2234
Residual elect. density (e$^-$ 10^{-6} pm^{-3})	3.8/−3.5	3.4/−2.9

2.2. Single crystal structure determination

For the crystal structure determinations, single crystals were selected using a stereo microscope and mounted in glass capillaries (diameter 0.1 mm) under dried paraffine oil. The crystals of silver metallic lustre were centered on a diffractometer equipped with an image plate detector.

Single crystals of the Au-rich compound $CaAu_{0.89}Cd_{0.11}$ showed the orthorhombic *C* centered lattice typical for the CrB structure type with the additional extinction condition '$h0l : l = 2n$' limiting the choice of space groups to *Cmcm* and $Cmc2_1$. The data could be refined using the program Shelxl-97 [18] to a low residual value *R* 1 of 3% starting from the crystal data of the isotypic binary auride CaAu [1] assuming a statistic occupation of the gold position with Au and Cd (final results see Tables 2 and 4 [19]).

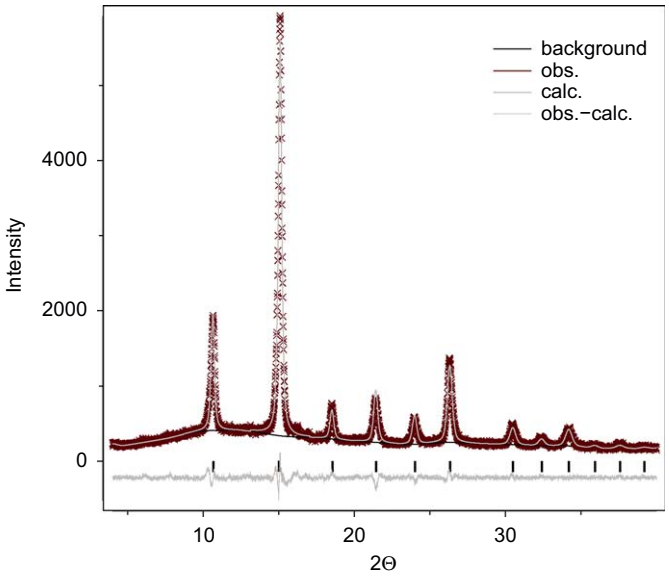

Fig. 1. Result of the Rietveld refinement of $CaAu_{0.29}Cd_{0.71}$ [25].

Table 4
Atomic coordinates and equivalent isotropic displacement parameters (pm^2) in (top down) $CaAu_{0.89}Cd_{0.11}$ (CrB type), $CaAu_{0.29}Cd_{0.71}$ and $CaAu_{0.13}Cd_{0.87}$ (CsCl type), $SrAu_{0.93}Cd_{0.07}$ and $SrAu_{0.78}Cd_{0.22}$.

Atom	Wyckoff position	Cd atoms	*x*	*y*	*z*	$U_{equiv.}$
Ca(1)	4*c*	–	0	0.3589(4)	1/4	334(14)
M(1)	4*c*	0.45(12)	0	0.07825(6)	1/4	322(4)
Ca(1)	1*a*	–	0	0	0	302(29)
M(1)	1*b*	0.71(2)	1/2	1/2	1/2	413(13)
Ca(1)	1*a*	–	0	0	0	365(24)
M(1)	1*b*	0.87(1)	1/2	1/2	1/2	425(16)
Sr(1)	2*e*	–	0.7442(3)	1/4	0.4534(2)	236(7)
Sr(2)	2*e*	–	0.8951(3)	1/4	0.1205(2)	240(7)
Sr(3)	2*e*	–	0.5828(3)	1/4	0.78686(19)	241(7)
M(1)	2*e*	0.15(4)	0.21926(13)	1/4	0.35917(8)	244(5)
M(2)	2*e*	0.13(5)	0.05812(13)	1/4	0.69158(8)	235(4)
M(3)	2*e*	0.16(4)	0.37450(13)	1/4	0.02517(8)	249(5)
Sr(1)	4*c*	–	0.14201(15)	1/4	0.0136(11)	396(13)
Sr(2)	4*c*	–	0.2677(2)	1/4	0.2485(10)	490(2)
Sr(3)	4*c*	–	0.39259(15)	1/4	0.0163(10)	383(13)
Sr(4)	4*c*	–	0.0179(2)	1/4	0.2465(6)	299(14)
M(1)	4*c*	0.88(12)	0.17806(7)	1/4	0.5120(5)	371(8)
M(2)	4*c*	0.48(16)	0.30232(12)	1/4	0.7527(3)	417(13)
M(3)	4*c*	0.58(13)	0.42835(6)	1/4	0.5103(5)	367(8)
M(4)	4*c*	1.51(15)	0.05370(11)	1/4	0.7491(4)	320(13)

The diffraction data of $SrAu_{0.93}Cd_{0.07}$ showed a monoclinic lattice with the additional systematic absence conditions 'reflections $0k0$ only present for $k=2n$' . The possible space groups ($P2_1/m$ and $P2_1$) and the lattice parameters are consistent with the structural model of $Y_{0.3}Gd_{0.7}Ni$ [10] with a h_2c stacking sequence of Ni zig-zag chains. The least squares refinement of the corresponding atomic coordinates applying anisotropic thermal parameters for all atom positions converged at a residual value of 0.047, whereat a small but significant Cd occupation is refined for all three crystallographic M positions. The crystallographic data and the refined atomic parameters are summarized in the Tables 3 and 4, respectively [19].

Crystals from a sample with slightly higher initial Cd content exhibit a primitive orthorhombic lattice, resembling the lattice parameter ratios and extinction conditions compatible with the space group *Pnma* of the $CaCu_{0.8}Zn_{0.2}$ type structure [14] with a $(h_3c)_2$ stacking. The data could be smoothly refined using the structure model of this compound, also applying a statistical occupation of the M positions. The crystal data and atomic parameters of this compound with the final composition $SrAu_{0.78}Cd_{0.22}$ are also collected in the Tables 3 and 4 [19].

2.3. Rietveld powder refinement

The compounds in the Cd-rich region of the section $CaAu_xCd_{1-x}$ could not be obtained in the form of crystals of adequate size and quality for a single crystal structure analysis. Therefore, the pure phase X-ray powder diagrams were used to refine the structure parameters applying the Rietveld method as implemented in the programs GSAS [20] and EXPGUI [21]. As depicted in Fig. 1 and listed in Table 2 the parameter refinements converged at good profile and structure R factors (for $x=0.29/0.13$) of $R_p=0.058/0.050$ and $R(F^2)=0.078/0.027$.

2.4. Band structure calculations

For the border compounds of the Ca series, CaAu and CaCd, as well as for the related compounds SrCd and BaZn, DFT calculations of the electronic band structures were performed using the FP-LAPW method (program WIEN2K [22]). The exchange-correlation contribution was described by the *Generalized Gradient Approximation* (GGA) of *Perdew*, *Burke* and *Ernzerhof* [23]. Muffin-tin radii were chosen as 121.7 pm (2.3 a.u.) for all atoms. Cutoff energies used are $E^{pot}_{max}=190$ eV (potential) and $E^{wf}_{max}=170$ eV (interstitial PW). Electron densities and *Fermi* surfaces were calculated and visualized using the programs XCRYSDEN [24] and DRAWXTL [25]. A *Bader* analysis of the electron density map was performed to evaluate the charge distribution between the atoms [26] and the bond critical points. In addition, the electron localization function (ELF) of CaCd was calculated using the program ELK [27]. Further details and selected results of the calculations are summarized in Table 6. The total and selected partial Au/Cd density of states are depicted in Fig. 4. The band structures of the elementary compounds CaCd (CsCl structure type) and CaAu (CrB structure type, [1]) are drawn along selected lines of the Brillouin zone in Figs. 5 and 6, respectively.

3. Results and discussion

3.1. Crystal structure description and comparison

The 1:1 polar intermetallic compounds exhibit a common structural chemistry: Like for the alkaline earth tetrelides (v.e./$M=6$), which can be (only formally) treated as electron precise Zintl compounds [3], the CrB type structure is also observed for many other less electron-rich compounds: CaGa (as the only trielide, 5), CaZn (4) [6], CaAg (3) [9] and CaAu (3) [1], etc. crystallize with this simple orthorhombic structure depicted on the left-hand side of Fig. 2. In the ideal CrB structure (orthorhombic, space group *Cmcm*, $a\approx c\approx 400$ pm and $b\approx 1100$ pm, cubic stacking exclusively) planar zig-zag chains of M atoms (M^{IV}, Ga, Zn, Ag, Au) running parallel to the c direction are stacked in identical orientation along the a axis. Every M atom is additionally coordinated by a trigonal prism of Ca/Sr atoms (shaded polyhedra in Fig. 2). One further alkaline earth atom completes this coordination sphere to 2+7. As known from several structural maps [11,13,15] the mono-tetrelides on one hand, and the electron poor compounds on the other hand have

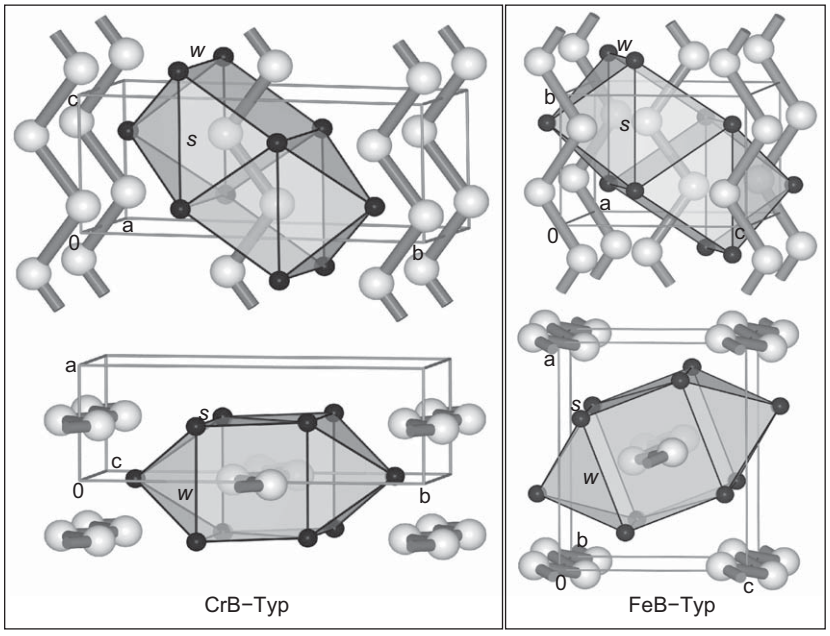

Fig. 2. Two different perspective views of the unit cells of the CrB (left) and the FeB structure type (right) (large light gray spheres: B/Au/Cd; small dark spheres Cr/Fe/Ca/Sr; [25]).

Table 5
Selected interatomic distances (pm) in $CaAu_{0.89}Cd_{0.11}$ (above), $SrAu_{0.93}Cd_{0.07}$ (middle) and $SrAu_{0.78}Cd_{0.22}$ (below).

Atoms	Distance	Mult.	CN	Atoms	Distance	Mult.	CN	Atoms	Distance	Mult.	CN
Ca(1)–*M*(1)	312.7(1)	4×		*M*(1)–*M*(1)	290.0(1)	2×					
Ca(1)–*M*(1)	316.5(3)	2×		*M*(1)–Ca(1)	312.7(1)	4×					
Ca(1)–Ca(1)	390.6(4)	4×		*M*(1)–Ca(1)	315.1(4)						
Ca(1)–Ca(1)	392.0(7)	2×		*M*(1)–Ca(1)	316.5(3)	2×	2+7				
Ca(1)–Ca(1)	397.7(2)	2×	6+8								
Sr(1)–*M*(1)	327.1(2)	2×		Sr(2)–*M*(2)	327.5(2)	2×		Sr(3)–*M*(3)	327.5(2)	2×	
Sr(1)–*M*(2)	327.4(2)	2×		Sr(2)–*M*(3)	328.7(2)	2×		Sr(3)–*M*(1)	328.3(2)	2×	
Sr(1)–*M*(2)	329.0(3)	2×		Sr(2)–*M*(3)	330.1(3)			Sr(3)–*M*(2)	330.1(3)		
Sr(1)–*M*(1)	329.3(3)			Sr(2)–*M*(3)	332.5(3)			Sr(3)–*M*(3)	331.4(3)		
Sr(1)–*M*(1)	332.3(3)			Sr(2)–*M*(3)	332.6(4)			Sr(3)–*M*(2)	332.5(3)		
Sr(1)–Sr(1)	401.2(4)	2×		Sr(2)–Sr(3)	405.9(3)	2×		Sr(3)–Sr(2)	405.9(3)	2×	
Sr(1)–Sr(3)	409.9(3)	2×		Sr(2)–Sr(3)	406.0(3)	2×		Sr(3)–Sr(2)	406.0(3)	2×	
Sr(1)–Sr(1)	411.2(4)	2×		Sr(2)–Sr(2)	409.8(4)	2×		Sr(3)–Sr(1)	409.9(3)	2×	
Sr(1)–Sr(2)	426.5(4)			Sr(2)–Sr(1)	426.5(4)			Sr(3)–Sr(2)	428.0(5)		
Sr(1)–Sr(3)	429.4(4)		8+8	Sr(2)–Sr(3)	428.0(5)		7+8	Sr(3)–Sr(1)	429.4(4)		7+8
M(1)–*M*(2)	294.5(1)	2×		*M*(2)–*M*(1)	294.5(1)	2×		*M*(3)–*M*(3)	293.6(1)	2×	
M(1)–Sr(1)	327.1(2)	2×		*M*(2)–Sr(1)	327.4(2)	2×		*M*(3)–Sr(3)	327.5(2)	2×	
M(1)–Sr(3)	328.3(2)	2×		*M*(2)–Sr(2)	327.5(2)	2×		*M*(3)–Sr(2)	328.7(2)	2×	
M(1)–Sr(1)	329.3(3)			*M*(2)–Sr(1)	329.0(3)			*M*(3)–Sr(2)	330.1(3)		
M(1)–Sr(1)	332.3(3)			*M*(2)–Sr(3)	330.1(3)			*M*(3)–Sr(3)	331.4(3)		
M(1)–Sr(2)	332.6(3)		2+7	*M*(2)–Sr(3)	332.5(3)		2+7	*M*(3)–Sr(2)	332.5(3)		2+7
Sr(1)–*M*(3)	329.1(4)	2×		Sr(2)–*M*(2)	328.3(6)	2×		Sr(3)–*M*(4)	328.3(4)	2×	
Sr(1)–*M*(4)	330.9(6)			Sr(2)–*M*(2)	330.2(7)			Sr(3)–*M*(1)	329.7(4)	2×	
Sr(1)–*M*(1)	333.3(7)			Sr(2)–*M*(1)	330.3(5)	2×		Sr(3)–*M*(3)	330.4(7)		
Sr(1)–*M*(2)	333.5(5)	2×		Sr(2)–*M*(1)	334.3(8)			Sr(3)–*M*(2)	336.1(6)		
Sr(1)–*M*(1)	335.2(7)			Sr(2)–*M*(2)	335.1(7)			Sr(3)–*M*(3)	337.4(7)		
Sr(1)–Sr(3)	407.1(9)	2×		Sr(2)–Sr(2)	409.2(5)	4×		Sr(3)–Sr(1)	407.1(9)	2×	
Sr(1)–Sr(3)	409.8(9)	2×		Sr(2)–Sr(1)	411.8(8)	2×		Sr(3)–Sr(1)	409.8(9)	2×	
Sr(1)–Sr(2)	411.8(8)	2×		Sr(2)–Sr(3)	430.4(9)			Sr(3)–Sr(4)	411.1(7)	2×	
Sr(1)–Sr(4)	428.1(9)			Sr(2)–Sr(1)	433.3(9)		7+8	Sr(3)–Sr(2)	430.4(9)		
Sr(1)–Sr(2)	433.3(9)		7+8					Sr(3)–Sr(4)	432.7(9)		7+8
Sr(4)–*M*(3)	329.3(5)	2×		*M*(1)–*M*(2)	294.3(2)	2×		*M*(2)–*M*(1)	294.3(2)	2×	
Sr(4)–*M*(4)	331.9(6)	2×		*M*(1)–Sr(3)	329.7(4)	2×		*M*(2)–Sr(2)	328.3(6)	2×	
Sr(4)–*M*(3)	332.0(7)			*M*(1)–Sr(2)	330.3(5)	2×		*M*(2)–Sr(2)	330.2(7)		
Sr(4)–*M*(4)	332.4(5)			*M*(1)–Sr(1)	333.3(7)			*M*(2)–Sr(1)	333.5(5)	2×	
Sr(4)–*M*(4)	335.4(5)			*M*(1)–Sr(2)	334.3(8)			*M*(2)–Sr(2)	335.1(7)		
Sr(4)–Sr(4)	406.3(7)	2×		*M*(1)–Sr(1)	335.2(7)		2+7	*M*(2)–Sr(3)	336.1(6)		2+7
Sr(4)–Sr(3)	411.1(7)	2×									
Sr(4)–Sr(4)	412.9(7)	2×									
Sr(4)–Sr(1)	428.1(9)										
Sr(4)–Sr(3)	432.7(9)		7+8								
M(3)–*M*(4)	293.9(2)	2×		*M*(4)–*M*(3)	293.9(2)	2×					
M(3)–Sr(1)	329.1(4)	2×		*M*(4)–Sr(3)	328.3(4)	2×					
M(3)–Sr(4)	329.3(5)	2×		*M*(4)–Sr(1)	330.9(6)						
M(3)–Sr(3)	330.4(7)			*M*(4)–Sr(4)	331.9(6)	2×					
M(3)–Sr(4)	332.0(7)			*M*(4)–Sr(4)	332.4(5)						
M(3)–Sr(3)	337.4(7)		2+7	*M*(4)–Sr(4)	335.4(5)		2+7				

vastly different geometrical proportions: In the electron-rich tetrelides the trigonal prisms are elongated (CrB-I type; prisms with a height versus basal lengths ratio $w/s > 1$) whereas at lower v.e.c. they show a compressed form (CrB-II; $w/s < 1$). Only CaGa and CaZn belong to an intermediate group with $w/s \approx 1$. For the border compound of the title series, CaAu [1], the Au–Au distances are 289.4 pm, the chain angle is 104.5° and $w/s = 0.86$. Up to 11% of Au can be substituted against Cd without significant structural changes ($d_{M-M} = 290.0$ pm; $\angle_{M-M-M} = 105.42(6)°$, selected atomic distances see Table 5).

The second closely related structure, the FeB type, is observed in some strontium and barium compounds with a v.e./M equal or below 4 (e.g. BaAg (3) [9,8] and SrZn (4) [1]). In this crystal structure shown on the right-hand side of Fig. 2, the zig-zag chains of the polyanions itself are unchanged with respect to the CrB structure. The planar chains are stacked in the hexagonal (h, after *Jagodzinski* [28]) orientation, meaning that the planes of the chains are tilt and the chains are separated from each other by the A cations. The monocapped trigonal-prismatic environment of M ($CN_M = 7$) is still very similar compared to the coordination in the CrB type structure. However, in the structures of the compounds with the bulky alkaline earth cations, the surrounding of M would be better described as a 6+1 coordination [9]. As for the CrB type structure, the more electron-rich compounds like LaSi [29] and LaGe [30] (v.e./$M = 7$) show stretched trigonal prisms around M, whereas the electron-poor compounds exhibit compressed prisms.

Although the FeB structure type is not observed in the title compound series, stacking variants in between the CrB and the FeB basic structures are observed around SrAg/SrAu und CaCu (cf. structure map in Fig. 7, Table 7 and discussion below). Starting from SrAu, which itself shows the complex stacking sequence $(hc)_2(h_2c)_2$ with 60% hexagonality [2] (Fig. 3 left), a successive change to structures with increased hexagonality is observed depending on the proportion of Cd substitution: In $SrAu_{0.93}Cd_{0.07}$ ($Gd_{0.7}Y_{0.3}Ni$ type [10], Fig. 3 middle) the stacking sequence is h_2c, i.e. the hexagonality increases to 66.7%. A slightly higher Cd content in $SrAu_{0.78}Cd_{0.22}$ drives the hexagonality to 75%, with the $(h_3c)_2$ stacking sequence also observed in the nearly isoelectronic compound $CaCu_{0.8}Zn_{0.2}$ [14] (right side of Fig. 3). Due to the small

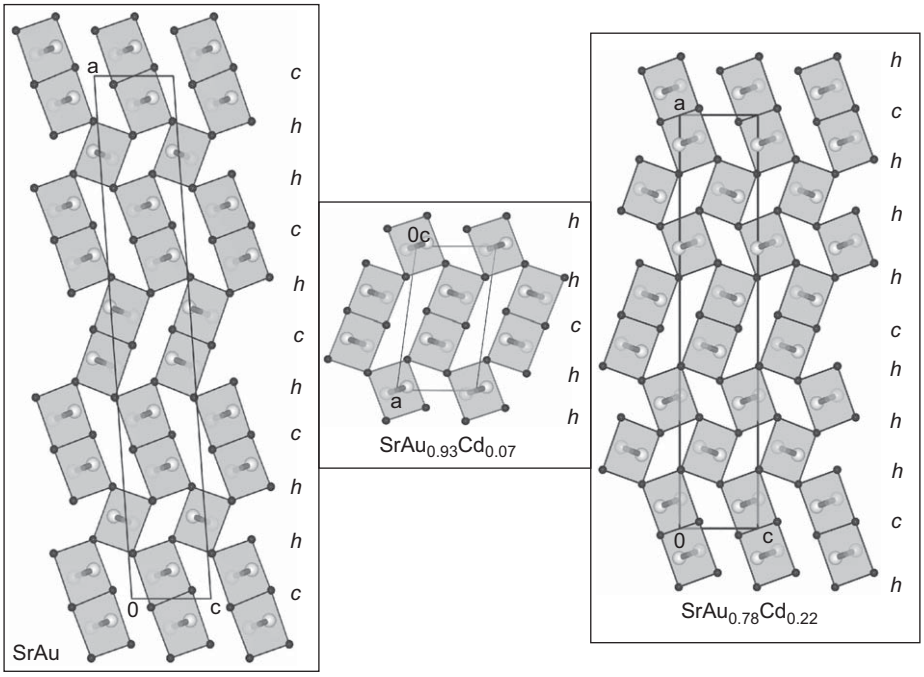

Fig. 3. View of the unit cells of SrAu (left), $SrAu_{0.93}Cd_{0.07}$ (middle) and $SrAu_{0.78}Cd_{0.22}$ (right) in a [010] projection (large light gray spheres: Au/Cd; small dark spheres Sr; [25]).

Table 6
Details of the calculation of the electronic structures of CaAu, CaCd, SrCd and BaZn.

		CaAu	CaCd	SrCd	BaZn
Structure type		CrB		CsCl	
Crystal data		[1]	[43]	[44]	[45]
R_{mt} (all atoms)		121.7 pm (2.3 a.u.)			
$R_{mt} \cdot K_{max}$		8.0			
k-Points/BZ		800		1000	
k-Points/IBZ		120		35	
Monkhorst-Pack-Grid		10 × 10 × 8		10 × 10 × 10	
DOS		Fig. 4	Fig. 4	–	–
Band structure		Fig. 6	Fig. 5	–	–
Electron density at BCP ($e^- 10^{-6}$ pm^{-3}) (d (pm))	Bond				
	M–M	0.299 (289.4)	0.0904 (383.9)	0.0774 (400.3)	0.0638 (409.3)
	M–A	0.138 (309.8)	0.0883 (332.5)	0.0877 (346.7)	0.0850 (354.5)
Bader charges	Au/Cd/Zn	−1.311	−1.233	−1.109	−0.950

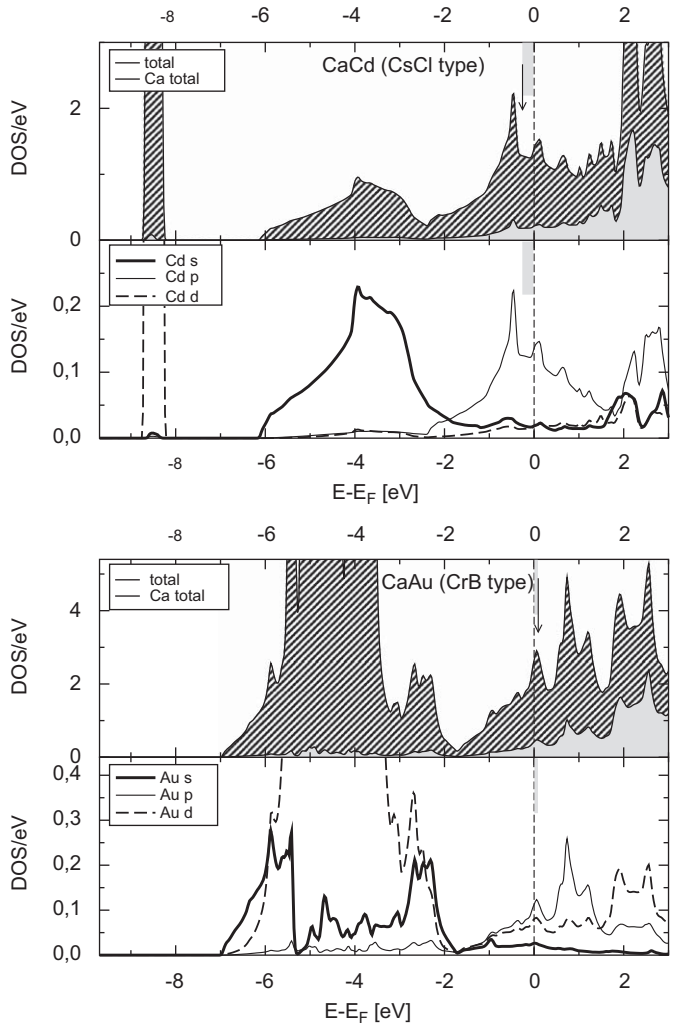

Fig. 4. Calculated total density of states (tDOS, above) together with (below) partial Cd/Au states (pDOS) of CaCd (above) and CaAu (below) in the range between −9.5 and 3 eV relative to the Fermi level E_F.

Cd content the *M*–*M* bond distances are very similar in these three Sr aurides ($d_{M-M} = 293.6 - 294.5$, see Table 5). The *M* positions in both ternary compounds are occupied by nearly equal amounts of Cd and Au, i.e. no distinct ordering of the two atom types is observed (Table 4). Due to the complicated crystal and thus also electronic structures, the change of the stacking in these very similar compounds is not easy to understand. Nevertheless, the changes observed when starting from Sr(Ag/Au) are parallel to the tendencies observed when starting from CaCu and CaAg (see discussion of the structural map below).

In addition to the CrB–FeB structure series, the CsCl/β−brass structure type occurs for polar 1:1 alkaline earth intermetallics at v.e./$M = 4$, in particular for compounds with a very large radius ratio r_M/r_A like (Ca/Sr)(Cd/Hg) at one hand and for BaZn with a very small r_M/r_A ratio on the other hand. In the Cd-rich part of the CaAu–CaCd section, this structure type occurs from CaCd up to a gold content of 29%. In accordance with the metallic radii of Au (144.2 pm, [31]) and Cd (156.8 pm) the unit cell volume decreases with increasing gold proportion. The observed phase width is discussed together with the calculated band structure of CaCd in the following section.

3.2. Electronic structure

The electronic structure of the two structurally simple border compounds of the series $CaAu_xCd_{1-x}$ together with the isotypic compounds SrCd and BaZn were calculated in the framework of the DFT method (cf. *Experimental section* and Table 6). The calculated total and partial Au and Cd density of states (tDOS/pDOS) of both binary border phases (Fig. 4) shows the expected metallic character of CaAu and CaCd and the next to complete electron transfer from Ca to Au/Cd, which causes Au to bear a charge of −1.33 and Cd of −1.23. The compounds can thus be addressed as 'cadmides' and 'aurides'. The electronic stability ranges, as observed via the Cd/Au substitution, are indicated as gray bars and arrows near the Fermi level in Figs. 4 (DOS), 5 and 6 (band structures).

The band structure of CaCd shown in the left-hand side of Fig. 5 is analogous to the textbook example of *p* bonded 'cubium'

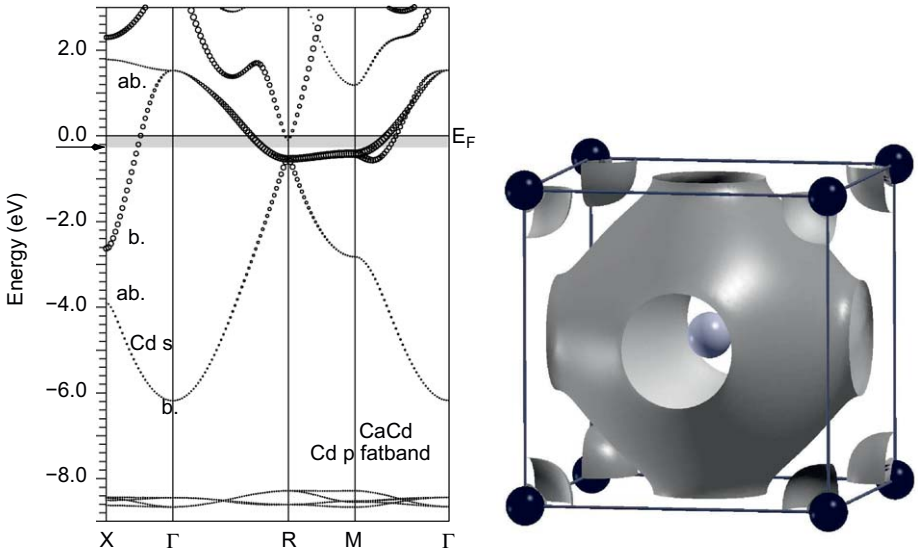

Fig. 5. Band structure of CaCd (in the Cd-*p* fat-band representation, left) and corresponding isosurface of the valence electron density drawn at a level of 0.08 $e^-/10^6$ pm^3 (right).

(α−Po type). As shown on the right-hand side of Fig. 5, the calculated valence electron density exhibits distinct bond critical points although in regions of low electron density between the Cd atoms. The band structure itself, especially the steep Cd *p*-like band between X $(\frac{1}{2},0,0)$ and Γ, the lower half being bonding, the upper half antibonding in character, indicates weak Cd–Cd p σ bonding contributions. The highest bond critical point in CaCd is thus found between Cd atoms, although the Cd–Cd distance is large (383.9 pm), in particular compared to the Ca–Cd contacts of 332.5 pm, which also exhibit saddle points in the calculated valence electron density map. The results are confirmed by a calculation of the electron localization function, which shows local maxima on the faces of the unit cell, which posses the cylindrical shape typical for σ bonds. Like in the tDOS plots of Fig. 4, the gray bar and the arrow in the bandstructure in Fig. 5 indicate the electronic stability range of the CsCl structure type experimentally probed by the substitution of cadmium against gold, both of similar electronegativity. Evidently, the limit of the Au substitution is reached at a v.e./*M* of 3.71, where the described $p-\sigma$ contribution becomes antibonding in character and the regions of higher total density of states, caused by the degenerate flat bands between R $(\frac{1}{2},\frac{1}{2},\frac{1}{2})$, representing the direction of the shortest Ca–Cd contact) and M $(\frac{1}{2},\frac{1}{2},0)$, are not yet depopulated. In the isotypic compound BaZn, where the difference in electronegativity between the two metals is less pronounced and where the radius ratio is very different (large *A* compared to small *M*, see structural map), the chemical bonding is significantly different: In this case, the $X \mapsto \Gamma$ band is located completely below E_F; the charge transfer from Ba to Zn is much less complete (Zn in BaZn −0.95 compared to −1.23 for Cd in CaCd), the highest bond critical points can be found between Ba and Zn and not between the Zn atoms. The weaker bonding in BaZn, when compared to all Cd/Hg compounds, is also evident from the melting points: BaZn has a melting point of only 340 °C, whereas all Cd and Hg compounds exhibit melting points above 600 °C. According to the geometrical and electronic situation (band structures, charge

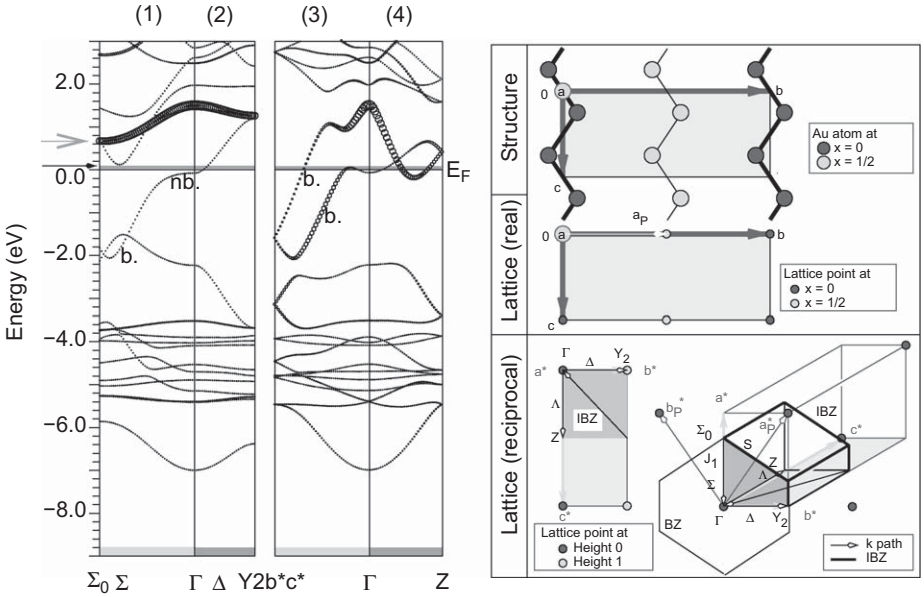

Fig. 6. Band structure of CaAu (in the Au-p_z fat-band representation, left) together with an explanation of the selected *k*-path.

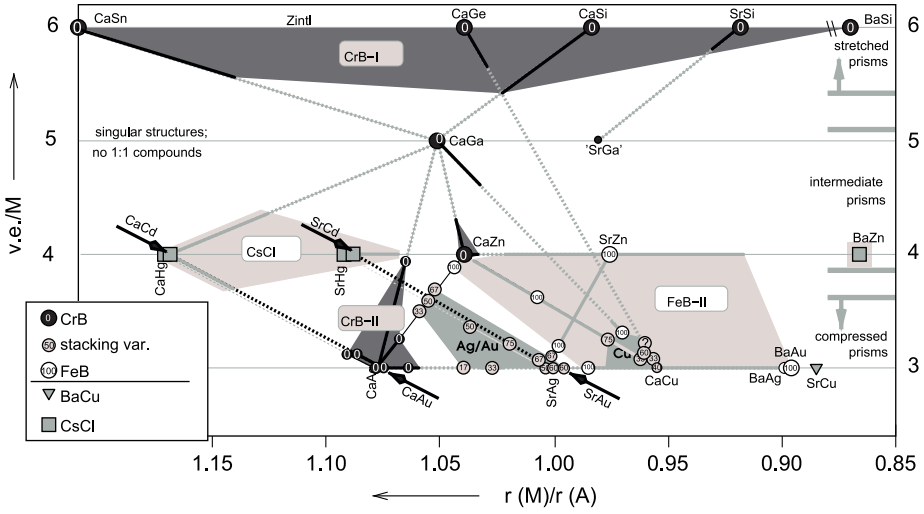

Fig. 7. Structural map of polar intermetallic 1:1 compounds with a v.e. number/*M* of 3 to 6. The title sections of this work CaCd–CaAu and SrCd–SrAu are marked with arrows.

Table 7
Binary and mixed ternary alkaline earth monometallides AM (M = group Ib, IIb, III and IV element; singular compounds AM^{III} and $AM_x^{III}M_{1-x}^{III}$ omitted).

Compound (series)	x	Ref.	Structure type	Stacking sequence	Hexagonality (%)	v.e./M
CaCu	–	[8]	α–CaCu	$(hch_2c)_2$	60	3
CaCu	–	[8]	β–CaCu	hc_2hc	40	3
SrCu, BaCu	–	[46]	BaCu	–	–	3
CaAg	–	[1]	CrB	c	0	3
$Ca_xSr_{1-x}Ag$	1–0.75	[9]	CrB	c	0	3
	0.48	[9]	new	(hc_5)	17	3
	0.39–0.25	[9]	HT-TbNi	$(hc_2)_2$	33	3
	0.05–0	[9]	SrAg	$(hc)_2$	50	3
SrAg	–	[8]	SrAg	$(hc)_2$	50	3
$Sr_xBa_{1-x}Ag$	0.84-0	[9]	FeB	h_2	100	3
BaAg	–	[8]	FeB	h_2	100	3
CaAu	–	[1]	CrB	c	0	3
SrAu	–	[2]	SrAu	$(hc)_2(h_2c)_2$	60	3
BaAu	–	[2]	FeB	h_2	100	3
$CaCu_xAg_{1-x}$	1–0.95	[14]	β–CaCu	hc_2hc	40	3
	0.90–0.70	[14]	$CaCu_{0.80}Ag_{0.2}$	$(hc_4)_2$	20	3
	0.65–0	[14]	CrB	c	0	3
$SrCu_xAg_{1-x}$	0.60–0.29	[32]	FeB	h_2	100	3
	0.11	[32]	α–CaCu	hc_2hc	40	3
$CaCu_xZn_{1-x}$	1–0.975	[14]	β–CaCu	hc_2hc	40	3.00–3.03
	0.95–0.85	[14]	HT-TbNi	$(hc_2)_2$	33	3.05–3.15
	0.85–0.70	[14]	$CaCu_{0.8}Zn_{0.2}$	$(h_3c)_2$	75	3.15–3.30
	0.65–0.05	[14]	FeB	h_2	100	3.35–3.95
$SrCu_xZn_{1-x}$	0.95–0.90	[32]	$SrCu_{0.9}Zn_{0.1}$	h_3chc	66.7	3.05–3.10
	0.85–0.20	[32]	FeB	h_2	100	3.15–3.80
$CaCu_xCd_{1-x}$	0.9	[16]	$CaCu_{0.975}Ga_{0.025}$	$(hc)_2(hc_2)_2$	40	3.10
$CaCu_xCd_{1-x}$	0.9	[16]	BaCu	–	–	3.10
	0.1	[16]	CsCl	–	–	3.90
$CaAg_xZn_{1-x}$	1–0.76	[15]	CrB	c	0	3.0–3.24
	0.52	[15]	HT-TbNi	$(hc_2)_2$	33	3.48
	0.48	[15]	SrAg	$(hc)_2$	50	3.52
	0.33	[15]	$Gd_{0.7}Y_{0.3}Ni$	h_2c	66.7	3.67
	0.14–0.05	[15]	FeB	h_2	100	3.86–3.95
$CaAg_xHg_{1-x}$	1–0.86	[47]	CrB	c	0	3.00–3.14
$SrAg_xHg_{1-x}$	1-0.64	[47]	SrAg	$(hc)_2$	50	3.00–3.36
$BaAg_xHg_{1-x}$	1–0.82	[47]	FeB	h_2	100	3.00–3.18
$CaAu_xCd_{1-x}$	1–0.89	This work	CrB	c	0	3.00–3.11
	0.29–0	This work	CsCl	–	–	3.71–4.0
$SrAu_xCd_{1-x}$	0.93	This work	$Gd_{0.7}Y_{0.3}Ni$	h_2c	66.7	3.07
	0.78	This work	$CaCu_{0.8}Zn_{0.2}$	$(h_3c)_2$	75	3.22
$CaCu_xGa_{1-x}$	0.975	[13]	$CaCu_{0.975}Ga_{0.025}$	$(hc)_2(hc_2)_2$	40	3.05
	0.95	[13]	HT-TbNi	$(hc_2)_2$	33	3.10
	0.925	[13]	α–CaCu	hc_2hc	40	3.15
	0.9–0.8	[13]	FeB	h_2	100	3.20–3.40
	0.2–0	[13]	CrB	c	0	4.60–5
$CaAg_xGa_{1-x}$	1-0.52	[47]	CrB	c	0	3.00–3.60
$SrAg_xGa_{1-x}$	1–0.85	[47]	SrAg	$(hc)_2$	50	3.00–3.30
$CaCu_xGe_{1-x}$	1–0.987	[13]	β–CaCu	hc_2hc	40	3.04
	0.975–0.90	[13]	?	?	?	3.08–3.30
	0.10–0	[13]	CrB	c	0	5.70–6.00
$CaCu_xSn_{1-x}$	1–0.95	[16]	β–CaCu	hc_2hc	40	3.00–3.15
	0.925	[16]	?	?	?	3.23
	0.83	[16]	$CaCu_{0.80}Ag_{0.2}$	$(hc_4)_2$	20	3.51
CaZn	–	[6]	CrB	c	0	4
$Ca_xSr_{1-x}Zn$	0–0.28	[32]	FeB	h_2	100	4
SrZn	–	[1]	FeB	h_2	100	4
$Sr_xBa_{1-x}Zn$	0.54	[32]	FeB	h_2	100	4
BaZn	–	[7]	CsCl	–	–	4
CaCd	–	[43]	CsCl	–	–	4
SrCd, BaCd	–	[48]	CsCl	–	–	4
CaHg	–	[49]	CsCl	–	–	4
SrHg	–	[50]	CsCl	–	–	4
BaHg	–	[51]	CsCl	–	–	4
$CaZn_xCd_{1-x}$	0.61	[32]	FeB	h_2	100	4
	0.18	[32]	CsCl	–	–	4
$CaCd_xGa_{1-x}$	1–0.64	[32]	CsCl	–	–	4
CaGa	–	[52,3]	CrB	c	0	5
$CaGa_xSi_{1-x}$	0.58–0	[3]	CrB	c	0	5.40–6.00
$CaGa_xSn_{1-x}$	0.59–0	[3]	CrB	c	0	5.40–6.00
$SrGa_xSi_{1-x}$	0.42–0	[47]	CrB	c	0	5.58–6.00
$SrGa_xSn_{1-x}$	0.82–0	[47]	CrB	c	0	5.86-6.00
$BaGa_xSi_{1-x}$	0.11–0	[47]	CrB	c	0	5.89–6.00
$BaGa_xSi_{1-x}$	0.17–0	[47]	CrB	c	0	5.83–6.00
CaSi	–	[36,39,38]	CrB	c	0	6

Table 7 (*continued*)

Compound (series)	*x*	Ref.	Structure type	Stacking sequence	Hexagonality (%)	v.e./*M*
CaGe	–	[36,53,38]	CrB	*c*	0	6
CaSn	–	[36,53,38]	CrB	*c*	0	6
CaPb	–	[36–38]	CrB	*c*	0	6
SrSi	–	[36,39,38]	CrB	*c*	0	6
SrGe	–	[54,36,38]	CrB	*c*	0	6
SrSn	–	[55,36,38]	CrB	*c*	0	6
SrPb	–	[36,38]	CrB	*c*	0	6
BaSi	–	[39,38]	CrB	*c*	0	6
BaGe, BaSn	–	[36,38]	CrB	*c*	0	6
BaPb	–	[56,38]	CrB	*c*	0	6

distribution and bond critical points, Table 6) SrCd adopts an intermediate position between CaCd (large radius ratio r_M/r_A, significant bonding *M*–*M* contacts) and BaZn (small r_M/r_A, no *M*–*M* bonding).

The two noble metal compounds CaAu and CaAg [9,15] exhibit very similar band structures (Fig. 6). Both compounds show strong covalent bonding in the *M* chains caused by Au/Ag *sp* hybrid bands in the chain direction (3), together with considerable contributions of the Au/Ag *d* states, which are significantly increased in energy when compared to the cadmides (Fig. 4). The *k*-path used for the analysis of the chemical bonding in the CrB type structure is depicted at the right-hand side of Fig. 6 and detailed in [9,15]. Due to the fact that hardly any p_x bands (perpendicular to the plane of the zig-zag chain) are populated (see *k* path section (1)), CaAu exhibits compressed prisms and no bonding is found perpendicular to the chains. The character of the Au–Au bonding is found in the section (3) of the selected *k*-path ($b^*c^* \mapsto \Gamma$), which corresponds to the bond direction in the chains: *s*–*p* mixing and large *d*-state contributions cause strong Au–Au bonding with short bond length (289.4 pm) and high electron densities at the respective bond critical points ($0.299\,e^-\,10^{-6}\,pm^{-3}$). The very small phase width $CaAu_xCd_{1-x}$ (cf. gray bar and arrow in Fig. 6) is obviously limited by size criteria, because in the pseudobinary system CaAg–CaGa (i.e. for a smaller *M* substituent) the electronic stability range reaches up to v.e./$M = 3.96$ ($CaAg_{0.52}Ga_{0.48}$ [32,33]). The corresponding energy level is marked by a gray arrow in the band structure plot of CaAu, which is very similar to that of CaAg [15,9]. The elongation of the prisms from 405.2 pm in CaAg ($w/s = 0.87$, compressed prisms, CrB-II) to 415.5 pm in $CaAg_{0.52}Ga_{0.48}$ is evidently correlated with the population of p_x states in (1). It is accompanied by a decrease of the Ag/Ga–Ag/Ga bond lengths and the *c* axis, which can be explained by the population of bonding *sp* states in (3) [32].

3.3. Structural map

Due to of the very similar and strong charge transfer from *A* to *M* (calculated charges of *M* in the CrB type structures: CaGe: −1.262, CaGa: −1.255, CaZn: −1.228, CaAg: −1.274, CaAu: −1.311 and also in CaCd with the CsCl type: −1.233) the main factors determining the crystal chemistry of polar alkaline earth monometallides are geometric parameters (radius ratio r_M/r_A) and the v.e. concentration (denoted as v.e./*M*). Like for the structure maps of mixed trielides AM_2 [34], cationic radii after Shannon [35] were used to asses the size of the *A* atoms and metallic radii after Gschneidner and Waber [31] were used for the *M* atoms. Fig. 7 shows the structure map containing the binary compounds characterized primarily in the groups of Fornasini and Merlo and in our own work (symbols: filled circles: CrB; open circles: FeB; gray circles: stacking variants between CrB and FeB type; squares: CsCl structure; triangles: BaCu type) together with several series of mixed crystals $A'_x A_{1-x}'' M$ and $AM'_x M_{1-x}''$ (dashed lines). All data used are in addition detailed in Table 7.

At a valence electron number per *M* atom (v.e./*M*) of 6, i.e. in the electronic regime, where *M* chains are formally electron precise when applying the Zintl concept, the CrB structure type is observed across the entire range of possible radius ratios, from CaPb ($r_M/r_A = 1.31$ [36–38]) on one hand to BaSi ($r_M/r_A = 0.82$ [39,38]) on the other hand. Evidently, the bonding in the chains is strong, due to additional $p_M - \pi$ contributions discussed in [3]. The chains are clearly separated from each other, the *A* prisms surrounding *M* are of stretched shape (CrB-I type). The phase widths of mixed ternary calcium tetrelides/gallides are depicted in Fig. 7 as dark lines running from the respective tetrelide towards CaGa. They reach a minimum of 5.58 v.e./*M* in the system CaSi–CaGa, rationalized by an analysis of the band structure and the chemical bonding in CaSi and CaGa [3]. At a v.e./*M* of 5, CaGa is the only compound crystallizing with the CrB structure type, with an intermediate ratio of height:basis ratio *w*/*s* of 0.96 for the trigonal prisms around *M*. CaGa exhibits no π bonding inside the Ga chains. Other binary 1:1 trielides are either not known (Al, Ga: [40,41]) or they form other more complicated structures (In: [4]). Ternary mixed trielides form variants of the CrB type, where the chains are of undulated shape [5]. For a v.e./*M* of 5 (CaGa) and 4 (CaZn), the CrB type is only observed in the small radius range between 1.04 and 1.06. The binary compound CaZn and the ternary phases $CaAg_xGa_{1-x}$ are the only examples for the occurrence of this type at a v.e. number of 4. For larger *A* cations, from $Ca_{0.52}Sr_{0.48}Zn$ to SrZn [1] and up to $Sr_{0.54}Ba_{0.46}Zn$ [32] the FeB structure type is formed. For much larger (Ca(Cd/Hg) and Sr(Cd/Hg) down to $SrZn_{0.18}Cd_{0.82}$) and much smaller (BaZn) radius ratios, the CsCl or β brass structure occurs at v.e./$M = 4$. As discussed above on the basis of the calculated band structure of CaCd, this structure type is only observed in a small valence electron region from 4.37($CaCd_{0.63}Ga_{0.37}$) to 3.71 ($CaAu_{0.29}Cd_{0.71}$). In the region of valence electron concentrations between 4 and 3, i.e. also in the course of this work, the structural chemistry is much more complex: In between the stability ranges of the CrB-II (around the line CaAg [15]–$CaAg_{0.52}Ga_{0.48}$ [32,33], dark gray field in Fig. 7) and the FeB type (light gray) a great variety of stacking variants combining elements of the CrB and the FeB structure type exists (medium gray regions around Sr(Ag/Au) and CaCu in Fig. 7). For all series in this region of the structural map, the proportion of hexagonal stacking (numbers in circles) increases with decreasing radius ratio r_M/r_A (CaAg–SrAg–BaAg [9], CaAg–CaCu [14], SrAg–SrCu [32]) and increases with increasing valence electron count v.e./*M* (SrAu–SrCd (this work), CaAg–CaZn [15], CaCu–CaZn [14], SrAg–SrZn [13], CaCu–CaGa [13]).

3.4. Conclusion

From the great richness of polar intermetallic phases of the composition 1:1, which cover the range from classical electron precise Zintl phases like the alkaline earth tetrelides up to the

electron poor mono-metallides of the coin metals, the present work highlights only a small but exemplary sample, compounds of the sections CaAu–CaCd and SrAu–SrCd. Starting from CaCd (4 v.e./*M*) the CsCl/*β* brass type is stable up to a limit of 3.71 v.e./*M* ($CaAu_{0.29}Cd_{0.71}$). This substitution limit corresponds to a broad minimum in the calculated density of states of the binary border phases CaCd and also matches the features of the associated respective bandstructure. On the other hand the CrB type of CaAu (3 v.e./*M*) is only preserved up to 3.11 v.e./*M*, a fact that can also be rationalized with the bandstructure of the matching border compound CaAu. With the significantly decreased radius ratios $r(M)/r(A)$ in the analogous section SrAu–SrCd, several stacking variants between the FeB and the CrB structure type are observed in the electron poor, gold rich section. The sequence of evidently electronically influenced stacking variants, characterized by the so-called hexagonality of the stacking of *M* zig-zag chains, is 60–67–75% with increasing valence electron number/Cd content. It is thus comparable to the 60–67–100% sequence along the section SrAg–SrZn, the 40/35–70–100% series of CaCu–CaZn and the 0–33–50–67–100% hexagonality sequence of the section CaAg–CaZn. In these cases, the complexity of the bandstructures does not allow an immediate rationalization of the different stacking variants. The example CaZn, for which the calculated total energies of the CrB and the FeB structure differ by only 0.5 kJ/mol, suggests that already very small differences in several parameters may result in structural changes. These results and the numerous known phases reported in the literature (Table 7) are consistently summarized in a structural map (Fig. 7), which takes the valence electron numbers and the radius ratios as relevant structure determining parameters into account. Nevertheless it is also apparent from the map that a number of other still unexplored pseudobinary sections can be systematically analysed to improve the structural map and hence our understanding of the parameters influencing the structure formation and stability of polar equiatomic intermetallics.

Acknowledgments

We would like to thank the *Deutsche Forschungsgemeinschaft* and the *Adolf-Messer-Stiftung* for financial support and Dr. Martin Kroeker for contributing to the theoretical work.

Appendix A. Supplementary data

Supplementary data associated with this article can be found in the online version at 10.1016/j.jssc.2009.10.027.

References

[1] F. Merlo, J. Less-Common Met. 86 (1982) 241.
[2] M.L. Fornasini, J. Solid State Chem. 59 (1985) 60.
[3] W. Harms, M. Wendorff, C. Röhr, J. Alloys Compds. 469 (2009) 89.
[4] M. Wendorff, C. Röhr, Z. Anorg. Allg. Chem. 631 (2005) 338.
[5] M. Wendorff, C. Röhr, Z. Naturforsch. 63b (2008) 804.
[6] M.L. Fornasini, F. Merlo, J. Less-Common Met. 79 (1981) 111.
[7] C.M. Yasarov, I.N. Ganiev, Metalli 5 (1997) 127.
[8] F. Merlo, M.L. Fornasini, Acta Crystallogr. B 37 (1981) 500.
[9] W. Harms, F. Burggraf, M. Daub, I. Dürr, C. Röhr, Z. Anorg. Allg. Chem. 643 (2008) 2255.
[10] K. Klepp, E. Parthé, Acta Crystallogr. B 36 (1980) 774.
[11] K. Klepp, E. Parthé, J. Less-Common Met. 85 (1982) 181.
[12] K. Klepp, E. Parthé, Acta Crystallogr. B 37 (1981) 495.
[13] F. Merlo, M.L. Fornasini, J. Less-Common Met. 119 (1986) 45.
[14] F. Merlo, M.L. Fornasini, J. Less-Common Met. 109 (1985) 135.
[15] W. Harms, V. Mihajlov, M. Wendorff, C. Röhr, Z. Naturforsch. 64b (2009) 1127.
[16] F. Merlo, M.L. Fornasini, J. Less-Common Met. 133 (1986) 225.
[17] W. Harms, I. Dürr, C. Röhr, Z. Naturforsch. 64b (2009) 471.
[18] G.M. Sheldrick, SHELXL-97—Program for the refinement of crystal structures, University of Göttingen, Germany, 1997.
[19] Further details on the crystal structure investigations are available from the Fachinformationszentrum Karlsruhe, Gesellschaft für wissenschaftlich-technische Information mbH, D-76344 Eggenstein-Leopoldshafen 2 on quoting the depository numbers CSD 421003 ($CaAu_{0.89}Cd_{0.11}$), CSD 421004 ($SrAu_{0.78}Cd_{0.22}$) and CSD 421005 ($SrAu_{0.93}Cd_{0.07}$), the names of the authors, and citation of the paper (E-mail: crysdata@fiz-karlsruhe.de).
[20] A.C. Larson, R.B.V. Dreele, GSAS—General structure analysis system, Los Alamos National Laboratory Report LAUR 86-748, 2000.
[21] B.H. Toby, J. Appl. Crystallogr. 34 (2001) 210.
[22] P. Blaha, K. Schwarz, G.K.H. Madsen, D. Kvasnicka, J. Luitz, WIEN2K—An Augmented Plane Wave and Local Orbital Program for Calculating Crystal Properties, TU Wien, Austria, 2006, ISBN3-9501031-1-2.
[23] J.P. Perdew, S. Burke, M. Ernzerhof, Phys. Rev. Lett. 77 (1996) 3865.
[24] A. Kokalj, J. Mol. Graphics Modelling 17 (1999) 176.
[25] L.W. Finger, M. Kroeker, B.H. Toby, J. Appl. Crystallogr. 40 (2007) 188.
[26] R.W.F. Bader, Atoms in Molecules. A Quantum Theory International Series of Monographs on Chemistry, Clarendon Press, Oxford, 1994.
[27] J.K. Dewhurst, S. Sharma, L. Nordström, F. Cricchio, ELK—The Elk—FP-LAPW Code (Vers. 0.9.279) (2009); 〈http://elk.sourcefourge.net〉.
[28] H. Jagodzinski, Acta Crystallogr. 7 (1954) 17.
[29] A. Raman, H. Steinfink, Acta Crystallogr. 22 (1967) 688.
[30] K.H.J. Buschow, J.F. Fast, Phys. Stat. Sol. 16 (1966) 467.
[31] W.B. Pearson, The Crystal Chemistry and Physics of Metals and Alloys, Wiley Interscience, 1972.
[32] W. Harms, Ph.D. Thesis, University of Freiburg, Germany, 2008.
[33] C. Röhr, Ph.D. Thesis, TH Darmstadt, Germany, 1990.
[34] W. Harms, M. Wendorff, C. Röhr, Z. Naturforsch. 62b (2007) 177.
[35] R.D. Shannon, Acta Crystallogr. A 32 (1976) 751.
[36] W. Rieger, E. Parthé, Acta Crystallogr. 22 (1967) 919.
[37] G. Bruzzone, F. Merlo, J. Less-Common Met. 48 (1976) 103.
[38] F. Merlo, M.L. Fornasini, J. Less-Common Met. 13 (1967) 603.
[39] A. Currao, J. Curda, R. Nesper, Z. Anorg. Allg. Chem. 622 (1996) 85.
[40] M.L. Fornasini, Acta Crystallogr. C 39 (1983) 943.
[41] B. Huang, J.D. Corbett, Inorg. Chem. 37 (1998) 5827.
[42] G.M. Sheldrick, SHELXS-97—Program for the Solution of Crystal Structures University of Göttingen, 1997.
[43] G. Bruzzone, Gazz. Chim. Ital. 102 (1972) 234.
[44] W. Köster, J. Meixner, Z. Metallk. 56 (1965) 695.
[45] G. Bruzzone, M. Ferretti, F. Merlo, J. Less-Common Met. 114 (1985) 305.
[46] M.L. Fornasini, F. Merlo, Acta Crystallogr. B 36 (1980) 1288.
[47] W. Harms, V. Mihajlov, M. Wendorff, C. Röhr, in preparation.
[48] R. Ferro, Acta Crystallogr. 7 (1954) 781.
[49] G. Bruzzone, F. Merlo, J. Less-Common Met. 32 (1973) 237.
[50] G. Bruzzone, F. Merlo, J. Less-Common Met. 35 (1974) 153.
[51] G. Bruzzone, F. Merlo, J. Less-Common Met. 39 (1975) 271.
[52] J.-T. Zhao, D. Seo, J.D. Corbett, J. Alloys Compds. 334 (2002) 110.
[53] P. Eckerlin, H.J. Meyer, E. Wölfel, Z. Anorg. Allg. Chem. 281 (1955) 322.
[54] A. Betz, H. Schäfer, A. Weiss, Z. Naturforsch. 22b (1967) 103.
[55] A. Widera, H. Schäfer, J. Less-Common Met. 77 (1981) 29.
[56] D.E. Sands, D.H. Wood, W.J. Ramsey, Acta Crystallogr. 17 (1964) 986.